Journal of Sound and Vibration (1997) **207**(4), 435–451

TUNING OF SIMULATED NATURAL FREQUENCIES FOR A FLEXIBLE SHAFT–MULTIPLE FLEXIBLE DISK SYSTEM

C.-W. LEE

Center for Noise and Vibration Control (*NOVIC*), *Department of Mechanical Engineering*, *Korea Advanced Institute of Science and Technology*, *Science Town*, *Taejon* 305-701, *Korea*

H. S. JIA

System Mechanics Group, *Mechanical Engineering Research Laboratory*, *Korea Electric Power Research Institute*, 103-16, *Munji-Dong*, *Yusung-Ku*, *Taejon* 305-380, *Korea*

C.-S. KIM

Samsung Advanced Institute of Technology, *Precision Mechanics Laboratory*, *P.O. Box* 111, *Suwon* 440-600, *Korea*

AND

S.-B. CHUN

Department of Environmental Engineering, *Kyung-In Women's College*, *Incheon* 407-050, *Korea*

(*Received* 13 *November* 1996, *and in final form* 25 *February* 1997)

The vibration of a flexible shaft coupled with multiple flexible disks is investigated by using a substructure synthesis technique with the assumed modes method to be compared with experimental results. According to the nature of coupling with the rotor, disk vibratory modes are classified into three groups: uncoupled disk modes with more than one nodal diameters, umbrella modes coupled with the shaft longitudinal vibrations and disk modes with a single nodal diameter coupled with the shaft bending vibrations. The natural frequencies and mode shapes for each group are calculated by employing different solution and tuning techniques. It is shown that the tuning technique is capable of accurately predicting the natural frequencies of the complicated coupled vibratory system.

1. INTRODUCTION

The shaft–disk assembly is an important machine component widely used in many industrial applications: turbine rotors, brake systems, computer hard disk drive spindle systems, etc. The most popular analytical model for such systems at present is the flexible shaft–rigid disk model. In another aspect, single flexible disks have attracted a lot of research interest since the famous early researches [1–3]. A single disk with inner clamped and outer free boundaries can be modelled as an elastic disk rigidly attached to a rigid shaft with rigid bearings. For the two models above, no flexible coupling effects exist between the disks and the shaft except the rigid rotation effects—the rotary inertia effect and the gyroscopic moments.

0022–460X/97/440435 + 17 $25.00/0/sv971199

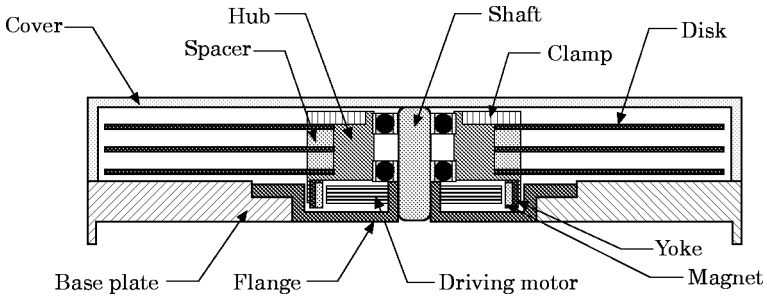

Figure 1. Cross-sectional view of the 3-disk HDD spindle system.

As the rotating systems become lighter and more flexible with higher operating speed for higher productivity and economical design, the flexible shaft-rigid disk model cannot accurately predict the vibration characteristics of some of these systems. Analytical models including disk flexibility have shown that in some situations it may significantly alter the vibration characteristics of the systems. Especially for the computer hard disk drive (HDD) spindle systems (Figure 1), due to the relatively large and thin disks, the disk flexibility will have important implications on the vibration properties of the spindle systems [4]. The rotordynamic analysis including disk flexibility is one area of current research interest. Since the coupled vibration of flexible shaft–disk systems is very complicated, for convenience in formulation, the total system will be classified into three groups according to the coupling nature in this research: uncoupled disk modes ($m \geqslant 2$), longitudinal coupled vibrations ($m = 0$) and bending coupled vibrations ($m = 1$) where m is the nodal diameter number of the disk modes. The uncoupled disk modes can be calculated by approximate methods [5]. No research paper has been found that addresses the problem of longitudinal coupled vibrations. Papers addressing the problems of the bending coupled vibrations are summarized in the next paragraph.

Dopkin and Shoup [6] analyzed the effect of disk flexibility and gyroscopic forces on the bending natural frequencies of an axisymmetric rotating shaft with multiple disks and bearings by a transfer matrix analysis. Chivens and Nelson [7] analytically investigated the influence of disk flexibility on the bending vibration using a flexible shaft, a rigid core and a flexible disk model. Wilgen and Schlack [8] applied the Liapunov method to an analytical model consisting of a flexible disk rigidly attached at an arbitrary location along a flexible shaft which is mounted on short, end bearings to investigate the effects of disk flexibility on the critical speeds. Shahab and Thomas [9] studied the coupling behavior between the stationary flexible thick discs and the flexible shaft carrying these discs by the finite element method and compared their calculated results with experimental results. Vance [10] considered the attachment flexibility of the disks to the shaft, and comparisons of numerical predictions with experimental measurements are shown. Wu and Flowers [11] developed a transfer matrix procedure in which the disk flexibility effects were accounted for by means of additional terms included in the transfer matrix formulation, and a continuous shaft with a single disk system was studied for the effect of disk flexibility.

The purpose of this paper is to present a method to calculate the natural frequencies of the complicated coupled vibrations of the HDD spindle systems (flexible shaft–multiple flexible disk systems)—both the longitudinal and bending coupled vibrations are included. This is a problem of importance in modern computer industry. Hard disk storage capacity is one of the most important characteristics of a computer. The data are stored

in concentric circular magnetic tracks on disks. The typical track density at present is about 4000 tpi (tracks per inch). The radial vibrations of disks is an obstacle to further increase of the track density for larger storage capacity. In addition, longitudinal vibrations of disks will interact with the read–write magnetic head, and excite head vibration and reduce the lifespan of the head–disk system. To reduce or control the vibrations of the spindle system, the natural frequencies need to be precisely predicted. Theoretical simulations are compared with experimental results, and then the original mathematical model is improved to "tune" the theoretical natural frequencies to the experimental ones.

2. THEORETICAL ANALYSIS

2.1. MODELLING

An analysis model consisting of a flexible shaft and N identical flexible disks rigidly attached to the shaft, as shown in Figure 2 is considered. It is assumed that the shaft is a beam with varying annular cross-section and each disk is a uniform circular plate. In modelling the flexible shaft, the rotary inertia and gyroscopic effects are taken into account. The disk model is described fully in reference [12]. In addition, small deformation is assumed throughout the analysis. The complicated coupled vibration of the flexible shaft–disk system will be analyzed. In particular, a few lowest vibration modes are of major interest. Tortional modes are not considered since no such modes are found in practical HDD spindle systems.

2.2. COUPLING CAUSED BY DISK FLEXIBILITY

To investigate the coupling caused by disk flexibility, a section (Figure 3) including one disk from the shaft–multiple disk system is chosen. One assumes that the attachment of the disk to the shaft is rigid, so that the disk remains normal to the shaft in all modes. For a rotating uniform disk, the eigenvalue problem for the elastic transverse vibration is self-adjoint, and it follows that its eigenfunctions constitute a complete set of orthogonal modes. Then, the flexible displacement of the elastic disk can be expressed according to

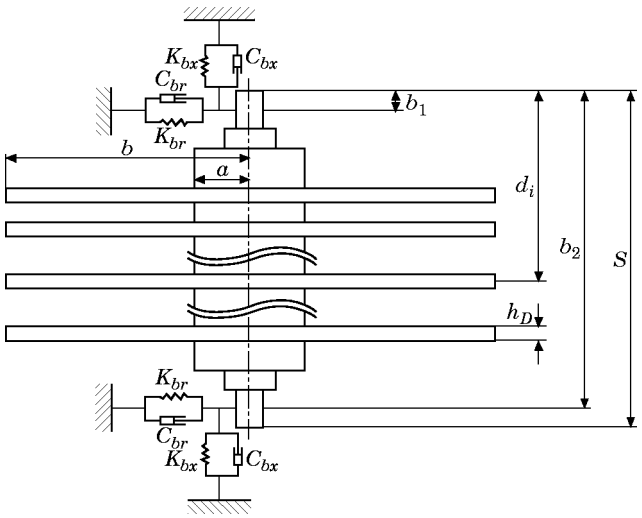

Figure 2. Analysis model.

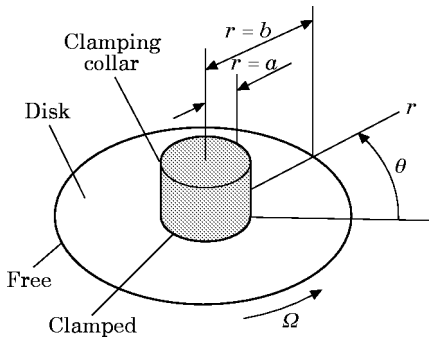

Figure 3. The co-ordinate system for coupling analysis.

the expansion theorem as

$$w(r, \theta, t) = \sum_{i=1}^{\infty} w_i(r, \theta) q_i(t)$$

where $w_i(r, \theta)$ are orthonormal modes of the disk, and $q_i(t)$ are the corresponding time-dependent generalized co-ordinates. Here harmonic vibration is considered, so that $\ddot{q}_i(t) = -\omega_i^2 q_i(t)$, where ω_i is the natural frequency of the ith disk mode. $w_i(r, \theta)$ may be expressed in the form [2]

$$w_i(r, \theta) = w_{mn}(r, \theta) = R_{mn}(r)(a_{mn} \cos m\theta + b_{mn} \sin m\theta), \qquad m, n = 0, 1, 2, \ldots, \infty$$

where $w_{mn}(r, \theta)$ represent the orthonormal modes of m nodal diameters and n nodal circles. $w_i(r, \theta)$ can be regarded as the reranking of $w_{mn}(r, \theta)$ by order of increasing corresponding natural frequencies. $R_{mn}(r)$ is the radial distribution of the mode shapes. a_{mn} and b_{mn} are constants determining the orientation angle θ_{mn0} of the resultant mode relative to the disk: $a_{mn} \cos m\theta + b_{mn} \sin m\theta = \cos m(\theta + \theta_{mn0})$.

The inertia force of the vibrating disk is

$$F = -\rho_D h_D \int_0^{2\pi} \int_a^b \frac{\partial^2 w}{\partial t^2} r \, \mathrm{d}r \, \mathrm{d}\theta$$

$$= -\rho_D h_D \sum_{i=1}^{\infty} \omega_i^2 q_i(t) \int_0^{2\pi} \int_a^b R_{mn}(r)(a_{mn} \cos m\theta + b_{mn} \sin m\theta) r \, \mathrm{d}r \, \mathrm{d}\theta$$

where

$$\int_0^{2\pi} (a_{mn} \cos m\theta + b_{mn} \sin m\theta) \, \mathrm{d}\theta = \begin{cases} 2\pi a_{0n}, & \text{for } m = 0 \\ 0, & \text{for } m \neq 0 \end{cases} \tag{1}$$

in which ρ_D and h_D are the mass per unit volume and thickness of the disk, respectively. The inertia moment to an arbitrary diameter (for example $\theta = \theta_0$) is

$$M_0 = -\rho_D h_D \int_0^{2\pi} \int_a^b \frac{\partial^2 w}{\partial t^2} r \sin(\theta - \theta_0) r \, \mathrm{d}r \, \mathrm{d}\theta$$

$$= -\rho_D h_D \sum_{i=1}^{\infty} \omega_i^2 q_i(t) \int_0^{2\pi} \int_a^b R_{mn}(r)(a_{mn} \cos m\theta + b_{mn} \sin m\theta) \sin(\theta - \theta_0) r^2 \, \mathrm{d}r \, \mathrm{d}\theta$$

where

$$\int_0^{2\pi} (a_{mn} \cos m\theta + b_{mn} \sin m\theta) \sin(\theta - \theta_0)\, \mathrm{d}\theta = \begin{cases} \pi(b_{1n} \cos\theta_0 - a_{1n} \sin\theta_0), & \text{for } m = 1 \\ 0, & \text{for } m \neq 1 \end{cases} \tag{2}$$

From equations (1) and (2), one knows that the disk modes of zero nodal diameter (umbrella modes) will have coupling with the longitudinal vibration of the shaft for the inertia force F, the disk modes of one nodal diameter will have coupling with the bending vibration of the shaft for the inertia moment M_0, and all other modes of nodal diameter $m \geqslant 2$ will have no coupling with the shaft vibration. Accordingly, in the following discussion, the vibration analysis will be divided into three groups: uncoupled disk vibration ($m \geqslant 2$), longitudinal (axial) coupled vibration ($m = 0$), and bending coupled vibration ($m = 1$).

2.3. ANALYSIS METHOD

A substructure synthesis technique with the assumed modes method [13] is used to investigate the coupled vibrations. The total system is regarded as an assemblage of substructures (flexible shaft and flexible disks). The energy elements for every substructure are determined by elastic deformations and fictitious boundary constraint conditions. The motion of every substructure may well be approximated by a weighted superposition of admissible functions. As admissible functions, the mode shapes obtained from the analytical solutions of individual non-rotating elements can be used. The energy elements are discretized by the introduction of admissible functions. For the uncoupled disk vibrations, only the assumed modes method is used. The Langrange equation is used then to formulate the equations of motion. The longitudinal and bending coupled governing equations are given in Appendix A and B separately. The eigenvalue problem associated with the equations can be easily formulated and solved [14]. A FORTRAN simulation program has been developed to calculate the natural frequencies and mode shapes of the uncoupled, longitudinal coupled and bending coupled vibrations. The method presented is computationally efficient and easy to use, and does not require the large number of degrees of freedom of the finite element analysis.

3. A NUMERICAL EXAMPLE

To demonstrate the proposed method, a commercial 3-disk HDD spindle system was selected as an example. To describe the local deflections of each elements, a total of 70 admissible functions (10 for each disk and shaft 2-DOF bending defections, and 20 for shaft axial defection) were used throughout the simulation. Mode shapes of the non-rotating uniform beam with free–free boundary conditions and the non-rotating uniform circular plate with inner clamped–outer free boundary conditions were used as the admissible functions for the shaft and the disks, respectively.

3.1. SIMULATION MODEL

The simulation model is a short hollow rotating spindle (hub) with three identical uniform disks and is simply supported by two ball bearings, as shown in Figure 4. The dimensional data according to Figure 4 are as follows (in mm): $r_1 = 6{\cdot}50$, $r_2 = 14{\cdot}00$, $r_3 = 14{\cdot}10$, $r_4 = 15{\cdot}30$, $r_5 = 16{\cdot}00$, $a = 16{\cdot}50$, $b = 47{\cdot}50$, $d_1 = 2{\cdot}40$, $d_2 = 5{\cdot}90$, $d_3 = 9{\cdot}40$, $h_D = 0{\cdot}80$, $h_1 = 10{\cdot}54$, $h_2 = 11{\cdot}09$, $h_3 = 14{\cdot}14$, $b_1 = 3{\cdot}50$, $b_2 = 12{\cdot}10$ and $S = 14{\cdot}79$. The

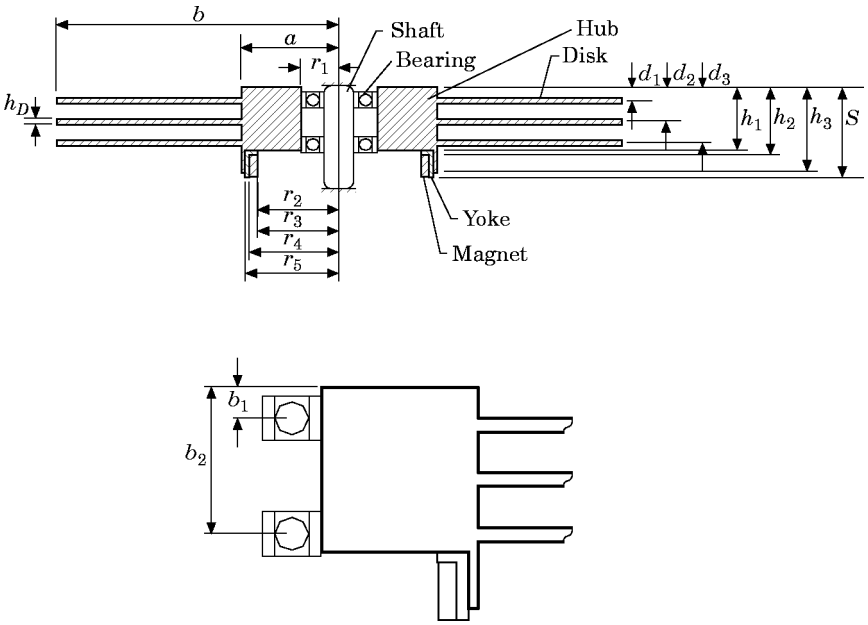

Figure 4. Cross-sectional view of the mathematical model.

material and bearing properties are: hub (flexible shaft) $\rho_S = 2750\ \text{kg/m}^3$, $E_S = 72{\cdot}0 \times 10^9\ \text{N/m}^2$, $v_S = 0{\cdot}3$; disk $\rho_D = 2800\ \text{kg/m}^3$, $E_D = 72{\cdot}0 \times 10^9\ \text{N/m}^2$, $v_D = 0{\cdot}36$; yoke $\rho_Y = 7800\ \text{kg/m}^3$, $E_Y = 204{\cdot}0 \times 10^9\ \text{N/m}^2$, $v_Y = 0{\cdot}3$; magnet $\rho_M = 5600\ \text{kg/m}^3$, $E_M = 72{\cdot}0 \times 10^9\ \text{N/m}^2$, $v_M = 0{\cdot}3$; bearing $K_{Bx} = 6 \times 10^6\ \text{N/m}$, $K_{Br} = 2 \times 10^7\ \text{N/m}$, $C_{Bx} = C_{Br} = 100\ \text{Ns/m}$. The denotations of parameters are given in Appendix D.

3.2. SIMULATION RESULTS

The natural frequencies of the axial coupled vibration of the 3-disk HDD spindle system are shown in Figure 5(a). The mode shapes of the first five modes are shown in Figure 6.

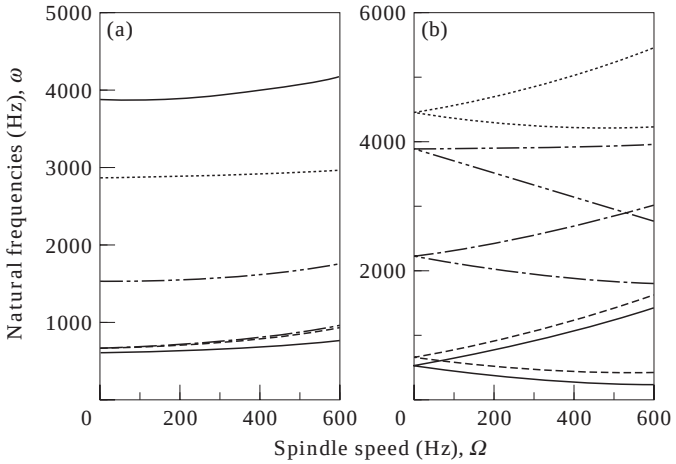

Figure 5. Natural frequencies of the coupled vibrations of the 3-disk HDD spindle system. (a) Axial coupled vibrations. (b) Bending coupled vibrations.

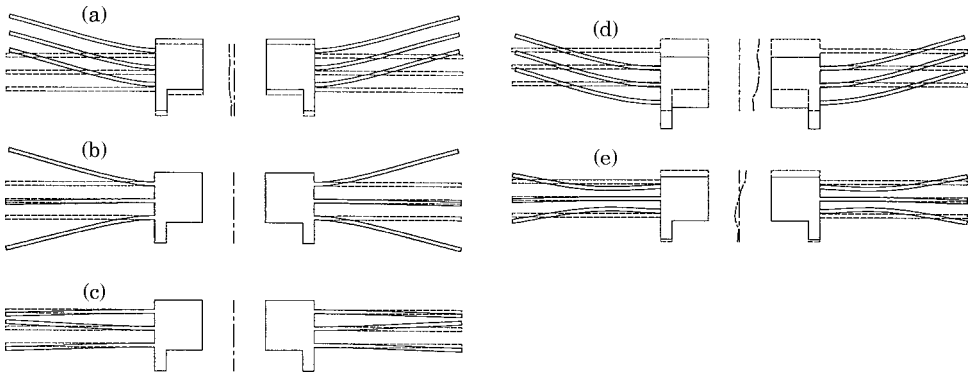

Figure 6. First five axial coupled vibration mode shapes of the 3-disk HDD spindle system.

The natural frequencies, relative to a stationary observer, of the bending coupled vibration of the 3-disk HDD spindle system are shown in Figure 5(b). The split of the natural frequencies into two branches $\omega_{1,2} = \omega_0 \pm m\Omega$ is typical of rotating disks where ω_0 is the frequency relative to rotating co-ordinates, Ω is the rotating speed and m is the nodal diameter number [15]. The mode shapes of the first five modes are shown in Figure 7. Note that in Figure 5(b), the second and third natural frequencies corresponding to modes (b) and (c) in Figure 7 cannot be separated from one another.

The normalized natural frequencies relative to a stationary observer of the 3-disk HDD spindle system are shown in Figure 8 where (m, n) is the disk mode with m nodal diameters and n nodal circles. The (0, 0) and (1, 0) modes are the longitudinal and bending coupled natural frequencies, respectively. The natural frequencies and rotor speed are scaled by the spindle nominal operating speed $\Omega_0 = 75$ Hz. The influences of shaft and disk flexibility on the natural frequencies are included. Figure 8(a) shows the results when both the shaft and the disks are rigid. Figure 8(b) shows the results when the disks are still rigid, but the shaft is flexible. Figure 8(c) shows the results when the shaft is rigid, but the disks are flexible. Figure 8(d) shows the results when both the shaft and the disks are flexible. From Figures 8(a) and (b), one can see that the shaft flexibility will reduce the longitudinal coupled natural frequency, but does not have any influence on the bending coupled vibration. In Figures 8(c) and (d), the lowest (0, 0) mode correspond to the axial vibration

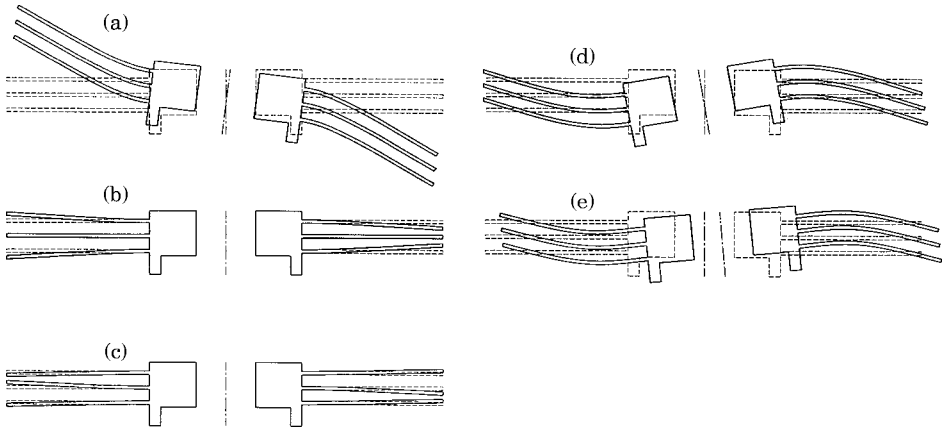

Figure 7. First five bending coupled vibration mode shapes of the 3-disk HDD spindle system.

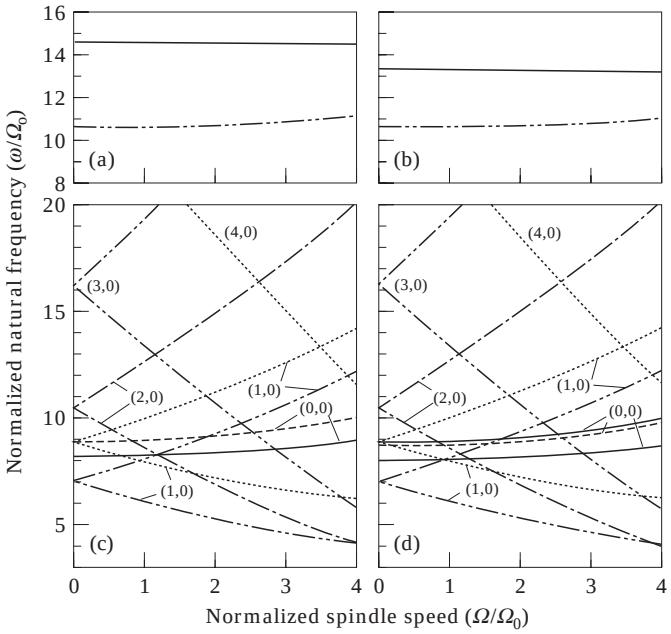

Figure 8. Natural frequencies of the 3-disk HDD spindle system: (a) rigid shaft + rigid disks; (b) flexible shaft + rigid disks; key for (a) and (b). ——, axial vibration; — · · — , bending vibration. (c) rigid shaft + flexible disks; (d) flexible shaft + flexible disks.

mode and the lowest (1, 0) mode correspond to the bending vibration mode in Figures 8(a) and 8(b), respectively. Comparing Figures 8(a) and (c), one concludes that the disk flexibility will have significant influence on both the longitudinal and bending coupled vibrations by reducing the values of the natural frequencies, introducing additional modes due to uncoupled disk vibrations and coupled vibrations and causing natural frequency splitting due to disk rotation. The results in Figure 8(d) are used to guide the HDD spindle system design.

Note that the natural frequencies described above are in the range of the disk transverse vibration. Figures 5–8 were drawn by using the tuned parameters in section 5.

4. EXPERIMENTAL APPARATUS AND METHOD

The experimental apparatus and instrumentation are depicted in Figure 9. Commercial 3-disk computer hard disk drives were tested when fixed onto a special vibration-isolation table. A gauging system with a capacitance type probe having a linear range of approximately 50·8 μm was used to measure the displacement of the upper disk without direct physical contact. The probe was fixed onto a stainless steel XYZ positioning stage. The disk was impacted by an impulse hammer instrumented with a piezoelectric force sensor. Displacement and force time records were input to a two-channel spectrum analyzer for frequency domain analysis. Peaks in the measured frequency response functions provided the system's natural frequencies. By transferring ensembles of measurements to a computer with a commercial experimental modal analysis package, the vibration modes of the HDD spindle system were determined through standard techniques. The modal testings were performed when the samples were at rest and in operation at 4500 rpm.

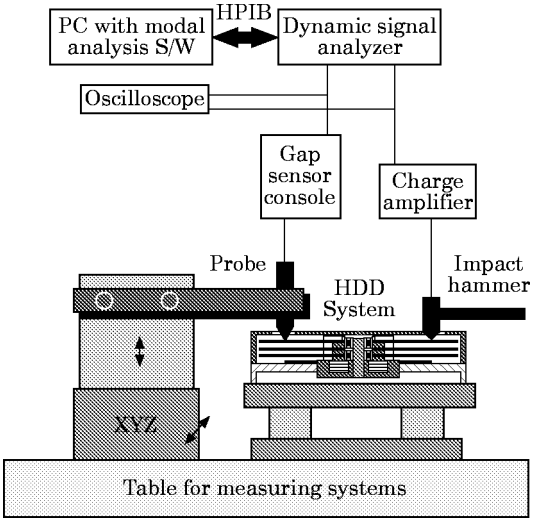

Figure 9. Schematic of the experimental apparatus.

5. TUNING OF SIMULATED NATURAL FREQUENCIES

Table 1 summarises the natural frequencies associated with the lower modes of the 3-disk HDD spindle system: the second column (Experiment 1) shows the average values from three test results, and the fourth to sixth columns (Simulation 1) give the untuned simulation results. Note that except for the conical (first bending coupled mode), (3, 0) and (4, 0) modes, the differences between the experimental and the simulation results are well over 5%. Thus in this section, an adequate tuning scheme will be sought so that the discrepancy between the simulated and the experimental results falls into an acceptable experimental error range. For this purpose, the disk modes and the axial coupled modes will be considered separately.

TABLE 1

Tuning of the simulated natural frequencies (Hz) *for the stationary* 3*-disk HDD spindle system*

			Simulation 1			Simulation 2		
Mode	Exp. 1†	Exp. 2‡	Freq. §	(S − E)‖	% Error	Freq.	(S − E)	% Error
Conical	526^{+2}_{-3}	517^{+7}_{-6}	528	2	0·38	517	−9	−1·71
Axial	549^{+1}_{-1}	592^{+2}_{-4}	652	103	18·76	549	0	0·00
Disk (0, 0)	615^{+3}_{-2}	618^{+5}_{-5}	672	57	9·27	610	−5	−0·81
(1, 0)	609^{+4}_{-4}	611^{+3}_{-6}	677	68	11·17	611	2	0·33
(2, 0)	721^{+4}_{-3}	726^{+4}_{-3}	781	60	8·32	717	−4	−0·55
(3, 0)	1162^{+8}_{-8}	1168^{+6}_{-5}	1199	37	3·18	1160	−2	−0·17
(4, 0)	1912^{+6}_{-8}	1918^{+6}_{-10}	1934	22	1·15	1916	4	0·21

† Exp. 1 = Average experimental frequency for real HDD spindle systems from three samples.
‡ Exp. 2 = Average experimental frequency for HDD spindle systems using rigid base.
§ Freq. = Simulated natural frequency.
‖ (S − E) = Simulated frequency − experiment 1.

TABLE 2

Comparison of the simulated natural frequencies (Hz) *by different methods*

Mode	$a/b = 0{\cdot}5$				$a/b = 0{\cdot}7$			
(m, n)	Simulation	V and S	(S − V)†	% Error	Simulation	V and S	(S − V)	% Error
(0, 0)	1138·1	1135·9	2·2	0·19	3228·9	3233·1	−4·2	−0·13
(1, 0)	1161·3	1162·2	−0·9	−0·08	3276·6	3276·8	−0·2	−0·01
(2, 0)	1285·2	1284·5	0·7	0·05	3432·0	3434·0	−2·0	−0·06
(3, 0)	1624·1	1616·5	7·6	0·47	3727·1	3722·4	4·7	0·13

† (S − V) = Simulated frequency − (V and S).

5.1. UNCOUPLED DISK MODES

From Table 1, it can be seen that the simulation results of the disk modes are larger than the experimental results. The natural frequencies of the stationary uncoupled disk are determined by

$$\omega_{mn} = \beta_{mn} \sqrt{D/(\rho_D h_D)}, \qquad D = E_D h_D^3/[12(1 - v_D^2)]$$

where D is called the flexural rigidity of the disk and β_{mn} is determined by a frequency determinant in which a and b are variants. For the stationary case, the ω_{mn} determined by this method is exact if the values of Bessel functions can be determined accurately. But the Bessel functions can only be determined approximately. Since the simulation results are larger than the experimental results, the mathematical model used should be improved. Before doing that, the accuracy of the simulation process will be confirmed first. Vogel and Skinner [16] calculated the natural frequencies of the stationary disk by replacing the Bessel functions with their approximate polynomial equivalents. The results (V and S) are listed in Table 2 together with the present simulation results for the stationary disk by the assumed modes method.

From Table 2, one can see that the results agree very well. Since the theoretical results in [16] agree within a few percent of the experimental results, one may use the simulation methods adopted here with confidence at least for the stationary disk.

Now one comes to the mathematical model used. The most possible cause of the discrepancies is the inner clamped boundary, especially because the thickness of the upper clamp being small (average thickness $\approx 1{\cdot}6$ mm), the rigid inner clamping model may be incorrect. The dimension of the clamp is shown in Figure 10(a). After the clamp is fixed, the dimension will change to Figure 10(b). One can see that the effective radius of the clamping will be smaller than the nominal radius. After choosing an effective inner clamping radius $a = 15$ mm instead of the nominal radius 16·5 mm for the upper disk, the

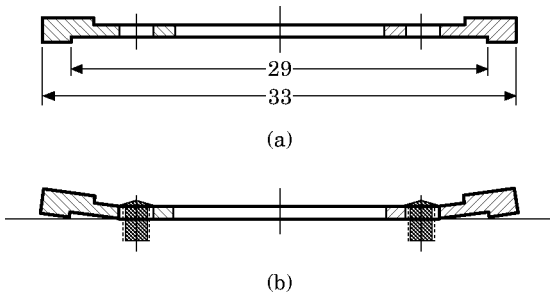

Figure 10. Dimension of the upper clamp (a) before and (b) after the clamping bolts are engaged.

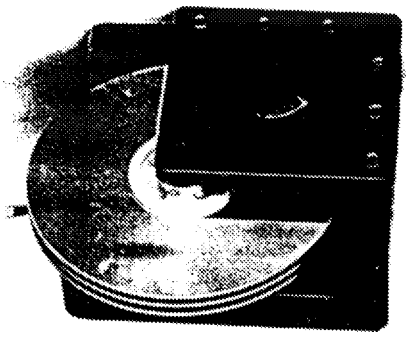

Figure 11. Rigid base.

results of Simulation 2 in Table 1 for the disk modes were obtained, and the errors are relative to Experiment 1. The results are in very good agreement.

5.2. THE AXIAL COUPLED MODE

The experimental natural frequency of the axial coupled mode is far less than the simulation result. The reduction of the natural frequency might be attributed to the cover and flange flexibility which are considered to be rigid in simulation (Figure 4).

Since the shaft–disk system is fixed to the upper cover and the lower flange (see Figure 1) which are made of the same material (aluminum) as the disk, and the cover and the flange have large area and small thickness, one can predict that their elastic deformation will have some influence on the axial coupled vibration and tend to reduce the longitudinal stiffness. To verify this prediction, a rigid base (Figure 11) was constructed. The rigid base still uses the real flange, but the upper cover has a much larger axial rigidity. The experimental results using the rigid base are given in Table 1 (Experiment 2). One can see that the natural frequency of the axial coupled mode apparently increases, but the influences on other natural frequencies are not apparent. This partly proves the authors' prediction. Now, one makes a simple calculation. The upper view of the cover is shown in Figure 12. P is the force of the spindle acting on the cover. The action of the spindle on the cover is approximated as a load P applied at the center of a simply supported square plate with side length $c = 100$ mm. Then the maximum deflection of the plate, which is at the center, is [17]

$$w_{max} = \alpha(Pc^2/D)$$

The effective stiffness is

$$K_c = D/\alpha c^2 = E_D\, h_D^3/[12(1 - \nu_D^2)\alpha c^2]$$

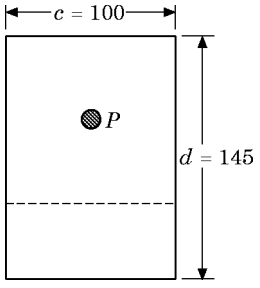

Figure 12. Upper view of the cover.

For a square plate, $\alpha = 0{\cdot}01160$, and $K_c = 4{\cdot}55 \times 10^5$ N/m. It is far less than the axial bearing stiffness ($K_{Bx} = 6 \times 10^6$ N/m). Since the cover and flange are difficult to model accurately, an effective axial stiffness $K_{Bxe} = 0{\cdot}85 \times 10^6$ N/m is introduced, to include the cover and flange flexibility in the simulation, in order to equate the calculated axial coupled natural frequency with the measured results when the disk is stationary. Since the effective clamping radius of the upper disk is 15 mm, an effective clamping radius for the coupled vibration modes is chosen as 16 mm ($=(15 + 16{\cdot}5 + 16{\cdot}5)$ mm/3). The tuned simulation result is listed in Table 1 (Simulation 2), and the error is relative to Experiment 1.

By using the effective radius for the coupled modes, the natural frequency of the conical mode is reduced, and its value is closer to the experimental result with the rigid base than to the result with the real base. The increase in natural frequency of this mode from the rigid base to the real base was found for all samples. It may be caused by flow–structure interaction. For the real base, the air was enclosed in the casing, and consequently it will have a large effect on the vibration. The simulation result which did not include the air effect should be closer to the experimental result of the rigid base rather than the real base. Hence simulation result using the effective clamping radius is more accurate, from the mathematical point of view, though it is farther from the experimental result of the real base.

From the description above, one obtained the tuned parameters:

(1) Disk modes, effective inner clamping radius $a = 15$ mm.

(2) Axial coupled vibration mode, effective inner clamping radius $a = 16$ mm and effective axial bearing stiffness $K_{Bxe} = 0{\cdot}85 \times 10^6$ N/m.

(3) Conical coupled vibration mode, effective inner clamping radius $a = 16$ mm.

Using these tuned parameters, one obtains the simulation results for both stationary and rotating cases as well as the experimental results in Table 3. The agreement between the theoretical and the experimental results are seen to be very good. The largest error is less than 2%.

TABLE 3

Tuning of the simulated natural frequencies (Hz) *for the* 3*-disk HDD spindle system*

	Stationary				4500 (r.p.m.)			
Mode	Exp.†	Simulation	(S − E)‡	% Error	Exp.	Simulation	(S − E)	% Error
Conical (b)	526^{+2}_{-3}	517	−9	−1·71	457^{+3}_{-7}	448	−9	−1·97
Conical (f)	—	—	—	—	605^{+5}_{-5}	598	−7	−1·16
Axial (0, 0)	549^{+1}_{-1}	549	0	0·00	555^{+5}_{-5}	552	−3	−0·54
Disk (0, 0)	615^{+3}_{-2}	610	−5	−0·81	621^{+2}_{-1}	615	−6	−0·97
(1b, 0)	609^{+4}_{-4}	611	2	0·33	543^{+2}_{-3}	543	0	0·00
(1f, 0)	—	—	—	—	692^{+1}_{-2}	693	1	0·14
(2b, 0)	721^{+4}_{-3}	717	−4	−0·55	583^{+6}_{-4}	577	−6	−1·03
(2f, 0)	—	—	—	—	882^{+3}_{-3}	877	−5	−0·57
(3b, 0)	1162^{+8}_{-8}	1160	−2	−0·17	949^{+9}_{-9}	943	−6	−0·63
(3f, 0)	—	—	—	—	1394^{+9}_{-9}	1393	−1	−0·07
(4b, 0)	1912^{+6}_{-8}	1916	4	0·21	1624^{+6}_{-8}	1624	0	0·00
(4f, 0)	—	—	—	—	2219^{+6}_{-8}	2224	6	0·27

† Exp. = Average experimental frequency for real HDD spindle systems from three samples.

‡ (S − E) = Simulated frequency − Exp.

6. CONCLUSIONS

A substructure synthesis technique with the assumed modes method has been developed to investigate the complicated coupled vibrations of a flexible shaft–multiple flexible disk system, and the theoretical results were compared with the experimental ones. The following conclusions from the investigation can be drawn for the HDD spindle systems with multiple flexible disks.

(1) The simulation and tuning techniques used are capable of accurately predicting the natural frequencies of the complicated coupled vibratory system. In particular, the conical (first bending coupled) natural frequency is precisely predicted. This mode is the most important mode of the 3-disk HDD spindle system. It is of greatest concern because it will cause read/write errors.

(2) The non-rigid clamping of the clamp and the cover and flange stiffness will have an important effect on the natural frequencies of the HDD spindle system.

(3) Natural frequencies are significantly influenced by disk flexibility.

(4) Shaft flexibility has little effect on the natural frequencies, except for the longitudinal coupled vibration.

ACKNOWLEDGMENT

The authors wish to acknowledge the Samsung Advanced Institute of Technology for supporting the research activity.

REFERENCES

1. G. R. Kirchhoff 1850 *Crelle's Journal* (*Jour. Math.*) **40**, 51–88. Über das Gleichgewicht und die Bewegung einer elastischen Scheibe; 1850 *Poggendorff's Annal* **81**, 258–264. Über die Schwingungen einer Kreisformigen elastischen Scheibe. Also see Lord Rayleigh 1945 *Theory of Sound* (two volumes). New York: Dover Publications, second edition. **1**, 352–394.
2. H. Lamb and R. V. Southwell 1921 *Proceedings of the Royal Society*, *London*, *Series A* **99**, 272–280. The vibration of a spinning disk.
3. R. V. Southwell 1922 *Proceedings of the Royal Society*, *London*, *Series A* **101**, 133–152. On the free transverse vibrations of a uniform circular disc clamped at its center; and on the effects of rotation.
4. C. W. Lee and S. B. Chun 1997 *American Society of Mechanical Engineers Journal of Vibration and Acoustics* **119**. Vibration analysis of a rotor with multiple flexible disks using assumed modes method.
5. C. D. Mote, Jr. 1970 *Journal of the Franklin Institute* **290**, 329–344. Stability of circular plates subjected to moving loads.
6. J. A. Dopkin and T. E. Shoup 1974 *American Society of Mechanical Engineers*, *Journal of Engineering for Industry* **96**, 1328–1333. Rotor resonant speed reduction caused by flexibility of disks.
7. D. R. Chivens and H. D. Nelson 1975 *American Society of Mechanical Engineers*, *Journal of Engineering for Industry* **97**, 881–886. The natural frequencies and critical speeds of a rotating, flexible shaft–disk system.
8. F. J. Wilgen and A. L. Schlack 1979 *American Society of Mechanical Engineers*, *Journal of Mechanical Design* **101**, 298–303. Effects of disk flexibility on shaft whirl stability.
9. A. A. S. Shahab and J. Thomas 1987 *Journal of Sound and Vibration* **114**, 435–452. Coupling effects of disc flexibility on the dynamic behavior of multi disc-shaft systems.
10. J. M. Vance 1988 *Rotordynamics of Turbomachinery*. New York: John Wiley; pp. 137–169.
11. F. Wu and G. T. Flowers 1992 *American Society of Mechanical Engineers*, *Journal of Vibration and Acoustics* **114**, 242–248. A transfer matrix technique for evaluating the natural frequencies and critical speeds of a rotor with multiple flexible disks.
12. H. S. Jia and C. W. Lee 1997 *Proceedings of the Second International Conference on Hydrodynamic Bearing–Rotor System Dynamics*, *Xi'an*, *China*, 199–204. Effects of imperfections in a rotating circular disk on its vibration characteristics.

13. L. MEIROVITCH 1980 *Computational Methods in Structural Dynamics*. The Netherlands: Sijthoff & Noordhoff; pp. 298–300 and 401–409.
14. C. W. LEE 1993 *Vibration Analysis of Rotors*. The Netherlands: Kluwer Academic Publishers; pp. 156–159.
15. S. A. TOBIAS and R. N. ARNOLD 1957 *Proceedings of the Institution of Mechanical Engineers* **171**, 669–690. The influence of dynamical imperfection on the vibration of rotating disks.
16. S. M. VOGEL and D. W. SKINNER 1965 *American Society of Mechanical Engineers*, *Journal of Applied Mechanics* **32**, 926–931. Natural frequencies of transversely vibrating uniform annular plates.
17. S. P. TIMOSHENKO and S. WOINOWSKY-KRIEGER 1959 *Theory of Plates and Shells*. Singapore: McGraw-Hill; pp. 141–143.

APPENDIX A: GOVERNING EQUATIONS OF THE LONGITUDINAL COUPLED VIBRATION

For the longitudinal coupled vibration of the shaft and disk umbrella modes, only longitudinal displacements need to be considered, and no gyroscopic moments and rotary inertia effect exist. The equations governing the longitudinal coupled vibration can be derived, based on substructure synthesis technique, as

$$\begin{bmatrix} \mathbf{m}_S & \mathbf{m}_{SD_1} & \cdots & \mathbf{m}_{SD_N} \\ \mathbf{m}_{SD_1}^{\mathrm{T}} & \mathbf{m}_D & 0 & \\ \vdots & 0 & \ddots & \\ \mathbf{m}_{SD_N}^{\mathrm{T}} & & & \mathbf{m}_D \end{bmatrix} \begin{Bmatrix} \ddot{\mathbf{Q}}_S \\ \ddot{\mathbf{Q}}_{D_1} \\ \vdots \\ \ddot{\mathbf{Q}}_{D_N} \end{Bmatrix} + \begin{bmatrix} \mathbf{m}_S & 0 & \cdots & 0 \\ 0 & 0 & 0 & \\ \vdots & 0 & \ddots & \\ 0 & & & 0 \end{bmatrix} \begin{Bmatrix} \dot{\mathbf{Q}}_S \\ \dot{\mathbf{Q}}_{D_1} \\ \vdots \\ \dot{\mathbf{Q}}_{D_N} \end{Bmatrix}$$

$$+ \begin{bmatrix} \mathbf{m}_S & 0 & \cdots & 0 \\ 0 & \frac{1}{2}(\mathbf{m}_D + \mathbf{m}_{\mathrm{D}}^{\mathrm{T}}) & 0 & \\ \vdots & 0 & \ddots & \\ 0 & & & \frac{1}{2}(\mathbf{m}_D + \mathbf{m}_{\mathrm{D}}^{\mathrm{T}}) \end{bmatrix} \begin{Bmatrix} \mathbf{Q}_S \\ \mathbf{Q}_{D_1} \\ \vdots \\ \mathbf{Q}_{D_N} \end{Bmatrix} = \begin{Bmatrix} 0 \\ 0 \\ \vdots \\ 0 \end{Bmatrix},$$

where

$$\mathbf{m}_S = \int_0^S \rho_S A_S \boldsymbol{\Phi}_S^{\mathrm{T}} \boldsymbol{\Phi}_S \, \mathrm{d}x + m_{D_0} \sum_{i=1}^{N} \boldsymbol{\Phi}_S |_{d_i}^{\mathrm{T}} \boldsymbol{\Phi}_S |_{d_i}, \qquad \mathbf{m}_D = 2\pi\rho_D h_D \int_a^b \boldsymbol{\Phi}_D^{\mathrm{T}} \boldsymbol{\Phi}_D \, r \, \mathrm{d}r,$$

$$\mathbf{m}_{SD_i} = 2\pi\rho_D h_D \, \boldsymbol{\Phi}_S^{\mathrm{T}}|_{d_i} \int_a^b \boldsymbol{\Phi}_D \, r \, \mathrm{d}r,$$

$$\mathbf{m}_S = \int_0^S E_S A_S \boldsymbol{\Phi}_S'^{T} \boldsymbol{\Phi}_S' \, \mathrm{d}x + K_{Bx} (\boldsymbol{\Phi}_S |_{b_1}^{\mathrm{T}} \boldsymbol{\Phi}_S |_{b_1} + \boldsymbol{\Phi}_S |_{b_2}^{\mathrm{T}} \boldsymbol{\Phi}_S |_{b_2}),$$

$$\mathbf{m}_D = 2\pi \int_a^b \left[Dr\boldsymbol{\Phi}_D''^{\mathrm{T}} \boldsymbol{\Phi}_D'' + 2Dv_D \boldsymbol{\Phi}_D''^{\mathrm{T}} \boldsymbol{\Phi}_D' + \left(N_r \, r + \frac{D}{r} \right) \boldsymbol{\Phi}_D'^{\mathrm{T}} \boldsymbol{\Phi}_D' \right] \mathrm{d}r,$$

$$\mathbf{m}_S = C_{Bx} (\boldsymbol{\Phi}_S |_{b_1}^{\mathrm{T}} \boldsymbol{\Phi}_S |_{b_1} + \boldsymbol{\Phi}_S |_{b_2}^{\mathrm{T}} \boldsymbol{\Phi}_S |_{b_2}).$$

$\boldsymbol{\Phi}_S$ is the row vector consisting of the admissible functions of the shaft, and $\mathbf{Q}_S$ is the column vector consisting of the corresponding time-dependent generalized co-ordinates; $\boldsymbol{\Phi}_D$ is the row vector consisting of the admissible functions of the disk and $\mathbf{Q}_{D_i}$ is the column vector consisting of the corresponding time-dependent generalized co-ordinates of the ith

disk. In addition, D is the flexural rigidity of the disk, N_r and N_θ are the normal centrifugal stress resultants in polar co-ordinates, and m_{D0} is the mass of a disk, which are all shown in Appendix C. Other parameters are defined in Appendix D.

APPENDIX B: GOVERNING EQUATIONS OF THE BENDING COUPLED VIBRATION

For the bending coupled vibration of the shaft and the single nodal diameter disk modes, in addition to the transverse displacements, the gyroscopic moments and the rotary inertia effect need to be considered. The bending coupled steady state equations resulting from the flexible shaft–disk model can be shown, based on substructure synthesis technique, to be

$$\begin{bmatrix} \mathbf{m}_S & -\mathbf{m}_{SD_1} & \cdots & -\mathbf{m}_{SD_N} \\ -\mathbf{m}_{SD_1}^{\mathrm{T}} & \mathbf{m}_D & 0 & \\ \vdots & 0 & \ddots & \\ -\mathbf{m}_{SD_N}^{\mathrm{T}} & & & \mathbf{m}_D \end{bmatrix} \begin{Bmatrix} \ddot{\mathbf{Z}}_S \\ \ddot{\mathbf{Z}}_{D_1} \\ \vdots \\ \ddot{\mathbf{Z}}_{D_N} \end{Bmatrix}$$

$$+ \begin{bmatrix} \mathbf{m}_S + \mathrm{j}\Omega(\mathbf{m}_S^{(1)} + \mathbf{m}_S) & 0 & \cdots & 0 \\ 0 & 0 & 0 & \\ \vdots & 0 & \ddots & \\ 0 & & & 0 \end{bmatrix} \begin{Bmatrix} \dot{\mathbf{Z}}_S \\ \dot{\mathbf{Z}}_{D_1} \\ \vdots \\ \dot{\mathbf{Z}}_{D_N} \end{Bmatrix}$$

$$+ \begin{bmatrix} \mathbf{m}_S^{(2)} + \mathbf{m}_S^{(3)} - \Omega^2\mathbf{m}_S^{(1)} + \mathrm{j}\Omega\mathbf{m}_S & -\Omega^2\mathbf{m}_{SD_1} & \cdots & -\Omega^2\mathbf{m}_{SD_N} \\ -\Omega^2\mathbf{m}_{SD_1}^{\mathrm{T}} & \tfrac{1}{2}(\mathbf{m}_D + \mathbf{m}_D^{\mathrm{T}}) & 0 & \\ \vdots & 0 & \ddots & \\ -\Omega^2\mathbf{m}_{SD_N}^{\mathrm{T}} & & & \tfrac{1}{2}(\mathbf{m}_D + \mathbf{m}_D^{\mathrm{T}}) \end{bmatrix} \begin{Bmatrix} \mathbf{Z}_S \\ \mathbf{Z}_{D_1} \\ \vdots \\ \mathbf{Z}_{D_N} \end{Bmatrix}$$

$$= \begin{Bmatrix} 0 \\ 0 \\ \vdots \\ 0 \end{Bmatrix}$$

where

$$\mathbf{m}_S = \int_0^S \rho_S \left(A_S\, \boldsymbol{\Phi}_S^{\mathrm{T}}\boldsymbol{\Phi}_S + I_S\, \boldsymbol{\Phi}_S'^{\mathrm{T}}\, \boldsymbol{\Phi}_S'\right) \mathrm{d}x + \sum_{i=1}^{N} \left(m_{D0}\, \boldsymbol{\Phi}_S\,|_{d_i}^{\mathrm{T}}\, \boldsymbol{\Phi}_S\,|_{d_i} + J_{Dy}\, \boldsymbol{\Phi}_S'\,|_{d_i}^{\mathrm{T}}\, \boldsymbol{\Phi}_S'\,|_{d_i}\right)$$

$$\mathbf{m}_D = \pi\rho_D\, h_D \int_a^b \boldsymbol{\Phi}_D^{\mathrm{T}}\boldsymbol{\Phi}_D\, r\, \mathrm{d}r, \qquad \mathbf{m}_{SD_i} = \pi\rho_D\, h_D\, \boldsymbol{\Phi}_S'\,|_{d_i}^{\mathrm{T}} \int_a^b \boldsymbol{\Phi}_D\, r^2\, \mathrm{d}r,$$

$$\mathbf{m}_S^{(1)} = \int_0^S \left(\rho_S\, A_S\, \boldsymbol{\Phi}_S^{\mathrm{T}}\boldsymbol{\Phi}_S - I_S\, \boldsymbol{\Phi}_S'^{\mathrm{T}}\, \boldsymbol{\Phi}_S'\right) \mathrm{d}x + \sum_{i=1}^{N} m_{D0}\, \boldsymbol{\Phi}_S\,|_{d_i}^{\mathrm{T}}\, \boldsymbol{\Phi}_S\,|_{d_i} + \sum_{i=1}^{N} (J_{Dy} - J_{Dx})\boldsymbol{\Phi}_S'\,|_{d_i}^{\mathrm{T}}\, \boldsymbol{\Phi}_S'\,|_{d_i},$$

$$\mathbf{m}_S^{(2)} = \int_0^S \left(E_S\, I_S\, \boldsymbol{\Phi}_S''^{\mathrm{T}}\, \boldsymbol{\Phi}_S''\right) \mathrm{d}x, \qquad \mathbf{m}_S^{(3)} = \sum_{i=1}^{2} K_{Br}\, \boldsymbol{\Phi}_S\,|_{b_i}^{\mathrm{T}}\, \boldsymbol{\Phi}_S\,|_{b_i},$$

$$\mathbf{m}_D = \pi \int_a^b \{Dr\boldsymbol{\Phi}_D''^{\mathrm{T}}\,\boldsymbol{\Phi}_D'' + 2Dv_D\boldsymbol{\Phi}_D''^{\mathrm{T}}\,\boldsymbol{\Phi}_D' + (N_r\, r + D(3-2v_D)/r)\boldsymbol{\Phi}_D'^{\mathrm{T}}\,\boldsymbol{\Phi}_D'$$
$$- (2Dv_D/r)\boldsymbol{\Phi}_D''^{\mathrm{T}}\,\boldsymbol{\Phi}_D - [2D(3-2v_D)/r^2]\boldsymbol{\Phi}_D'^{\mathrm{T}}\,\boldsymbol{\Phi}_D + (N_\theta\,/r + D(3-2v_D)/r^3)\boldsymbol{\Phi}_D^{\mathrm{T}}\boldsymbol{\Phi}_D\}\,\mathrm{d}r,$$

$$\mathbf{m}_S = \sum_{i=1}^{2} C_{Br}\,\boldsymbol{\Phi}_S\,|_{b_i}^{\mathrm{T}}\,\boldsymbol{\Phi}_S\,|_{b_i}$$

and

$$\mathbf{Z}_S = \mathbf{Q}_V + \mathrm{j}\mathbf{Q}_W, \qquad \mathbf{Z}_{D_i} = \mathbf{Q}_{\xi i} + \mathrm{j}\mathbf{Q}_{\eta i},$$

in which $\mathbf{Q}_V$ and $\mathbf{Q}_W$ are the column vectors consisting of the time-dependent generalized co-ordinates describing the shaft motion in two orthogonal planes, separately; and $\mathbf{Q}_{\xi i}$ and $\mathbf{Q}_{\eta i}$ are the column vectors consisting of the time-dependent generalized co-ordinates describing the degenerate "cosine" and "sine" modes of the ith disk, separately. Here, two orthogonal generalized co-ordinates take the real and imaginary parts of a generalized complex co-ordinate. In addition, I_S is the area moment of inertia of the shaft cross-section about a diameter; and J_{Dx} and J_{Dy} are the disk mass moments of inertia about the axis of rotation and a diameter, respectively; and K_{Br} and C_{Br} are the radial stiffness and damping of the bearings.

APPENDIX C: STRESSES, DISK MASS AND FLEXURAL RIGIDITY

$$N_r = \frac{\rho_D\, h_D\, \Omega^2}{8}\left[-(3+v_D)r^2 + C_1 + C_2\frac{1}{r^2}\right],$$

$$N_\theta = \frac{\rho_D\, h_D\, \Omega^2}{8}\left[-(1+3v_D)r^2 + C_1 - C_2\frac{1}{r^2}\right],$$

$$C_1 = \frac{(1+v_D)\,(3+v_D)b^4 + (1-v_D^2)a^4}{(1+v_D)b^2 + (1-v_D)a^2}, \qquad C_2 = b^2a^2\,\frac{(1-v_D)\,(3+v_D)b^2 - (1-v_D^2)a^2}{(1+v_D)b^2 + (1-v_D)a^2},$$

$$m_{D0} = \int_0^{2\pi}\int_a^b \rho_D\, h_D\, r\,\mathrm{d}r\,\mathrm{d}\theta = \pi\rho_D\, h_D\,(b^2 - a^2), \qquad D = \frac{E_D\, h_D^3}{12(1-v_D^2)}.$$

APPENDIX D: NOMENCLATURE

a	disk inner-clamping radius
A_S	cross-sectional area of the shaft
b	disk outer radius
C_{Bx}, C_{Br}	axial and radial damping coefficients of bearings
D	flexural rigidity of the disk
E_D, E_S, E_Y, E_M	Young's moduli
h_D	thickness of the disk
I_S	area moment of inertia of shaft cross-section about a diameter
J_{Dx}, J_{Dy}	disk mass moments of inertia about the rotating axis and a diameter
K_{Bx}, K_{Br}, K_{Bxe}	axial, radial and effective axial stiffness of bearings
m, n	disk mode (nodal diameters, nodal circles)
m_{D0}	mass of a disk
N	total number of disks
N_r, N_θ	stress resultants
q_i, $\mathbf{Q}_{Di}$, $\mathbf{Q}_S$, $\mathbf{Q}_V$, $\mathbf{Q}_W$, $\mathbf{Q}_{\xi i}$, $\mathbf{Q}_{\eta i}$	generalized co-ordinates

r, θ	polar co-ordinates for a disk
S	length of the flexible shaft
$\mathbf{Z}_S, \mathbf{Z}_{Di}$	generalized co-ordinates of complex form
$\mathbf{\Phi}_D, \mathbf{\Phi}_S$	row vectors consisting of admissible functions
$\rho_D, \rho_S, \rho_Y, \rho_M$	mass densities (per unit volume)
$\nu_D, \nu_S, \nu_Y, \nu_M$	Poisson's ratios
Ω	rotational speed of the shaft
Ω_0	nominal operating speed of the spindle

Subscripts

B	bearing
b_i, d_i	values evaluated at the ith bearing and ith disk location
D	disk
D_i	ith disk
M	magnet
S	shaft (hub)
Y	yoke